X-31 Vector Aircraft, Low Speed Stability & Control, Understanding from Comparing Wind Tunnel Data & Theory

Dr. R. K. Nangia & Dr M.E. Palmer

Nangia Aero Research Associates, WestPoint, 78-Queens Road, Clifton, BRISTOL, BS8 1QU, UK

Keywords: X-31 Vector, Canard -Wing Aircraft, Stability & Control, Aerodynamic Methods, Wind Tunnel Data

ABSTRACT

One of the NATO RTO-AVT Tasks is aimed at assessment of Stability and Control Prediction Methods for NATO Air and Sea Vehicles (essentially complex configurations). The assessments need to include the absolute values of forces and moments as well as the various symmetric and asymmetric stability derivatives, both steady and unsteady. This paper relates to the topic of the canard-delta X-31 "Vector" aircraft.

Low speed experimental data is from an X-31 model tested by DLR. The main focus of this paper is in the use of linear theory and Surface Singularity methods (Panel codes). Results are compared with experiment and other CFD methods. The main emphasis is on longitudinal stability aspects with component contributions. However, selected asymmetric effects are also considered.

For the symmetric cases, the predictions have shown good agreement for Lift with experiment and CFD up to α about 15°. For pitching moment, agreement with other CFD results is good up to α of 15°. The experiments show a more discontinuous behaviour beyond α about 10°. A series of longitudinal stabilty derivatives have been derived from the results. Longitudinal Trimming aspects are briefly discussed.

For the asymmetric cases with sideslip, a limited set of stability derivatives have been obtained. These are reasonable but need to be compared with experiments.

Work is needed for estimating roll / yaw derivatives.

The work so far has been interesting and encouraging. It has led to an improved understanding of the complex configurations with strongly interacting and separating / vortical flows. It is remarkable that low-order theories apply reasonably well up to α of 15° or so, with results being comparable with high-order CFD solvers.

In a wider future perspective, an understanding has evolved for either exploitation or avoidance of the complex flows. This is an important motivation.

1. INTRODUCTION

This paper arises from NATO RTO-AVT-161 task group initiative. The task group is aimed at the assessment of Stability and Control Prediction Methods for the NATO Air and Sea Vehicles (essentially complex configurations). The assessments need to include the absolute values of forces and moments as well as the various symmetric and asymmetric stability derivatives, both steady and unsteady. This paper relates to the topic of the canard-delta X-31 "Vector" aircraft.

The X-31 was designed and constructed as a demonstrator aircraft by Rockwell International Corporation's North American Aircraft and Deutsche Aerospace. The X-31 had a wing span s of 23.83 ft and a fuselage length of 43.33 ft. It was powered by a single GE F404-GE-400 turbofan (18,000 lb thrust in after-burn).

Fig.1 shows the layout of the X-31. Pertinent data on the wind tunnel model is in **Table 1** (see Ref.1). Some views of the model as per CATIA CAD-IGES geometry are in **Fig2**. It is worth noting that for trim condition at high AoA and low speeds the canard will be deflected down and TE flap up. **Fig.3** shows the CATIA model with a belly sting. **Fig.4** shows views of the Remote Control model with the rear sting support. **Fig.5** refers to the IGES geometry files and sections etc. Discontinuities in the IGES data were noted.

The wing planform has inboard LE sweep of 57°. Outboard of $\eta = 0.65$ the LE sweep is 45°. The TE is swept forward at about 10°. The wing root / fuselage side is at $\eta = 0.168$. The Canard LE and TE sweeps are 45° and 6° respectively. The reference setting for the canard is $\theta = 0°$. In flight, as wing angle of attack increases, the canard setting will reduce appropriately so as to keep lift on the canard fairly low. Such control aspects are not addressed.

Experimental data on a model with a wingspan of 1.0m is available from Ref.1. Tests were carried out at a nominal airspeed of 60 m/s (maximum 75 m/s). Assuming atmospheric conditions at Sea Level, 60 m/s corresponds to Mach 0.176. Typical graphs are shown in **Figs.6-7**. Some of these and others will be used in the comparisons.

We are focussing primarily on using linear theory and Surface Singularity methods (panel codes) to assess their applicability on this class of configuration. The emphasis is on longitudinal stability aspects. However, consideration will be given to selected asymmetric effects also.

2. MODEL DISCRETISATION

From the outline planforms, **Fig.8** and CATIA-IGES geometry, we have derived a discretised representation. This is based on our previous experience on such aircraft, Refs.2-4. **Fig.9** shows the panelling developed for the complete aircraft. The intake was faired over as in the experimental model. Note the inclusion, in the modelling, of the forward and aft body-side (wing root) strakes It needs to be mentioned that the CAD geometry had some inconsistencies near the leading and trailing edges and these had to be removed, virtually by hand. However, such an experience is not unique. We have often found this in other CAD descriptions.

To gain an understanding, we have studied the aircraft component build up, with and without the fuselage. This allows an assessment of the relative contributions to the various forces, moments and stability derivatives. The configuration has therefore been progressively represented using the following components, wing, canard, front and rear fuselage strakes, fin and fuselage. The thrust vectoring "paddles" (Vector Panels) have not been represented (as in

the wind tunnel tests). Mounting is assumed to be via a rear sting with loads on the sting discounted.

We consider first, symmetric longitudinal modes. Some CFD results for the complete configuration, using a Navier-Stokes solver were available from (Ref.5).

3. LONGITUDINAL STABILITY, WING + CANARD (NO FUSELAGE)

To understand the relative significance of the two lifting surfaces, initial assessments were carried out with the canard + wing configuration, **Fig.10**.

Fig.11 shows the spanwise loadings with canard set at $\theta = -5^o, 0^o, +5^o$. Wing and Canard contributions to total C_L and C_m are shown in **Fig.12** and compared with experiment. As the canard setting angle is reduced ($+5^o$ to -5^o), its C_L contribution decreases. These effects are evident in the spanwise loadings, **Fig.11**. We have attempted to show the possible reasons for breakpoints in the C_L and C_m trends. This type of analysis is extremely important for evaluating performance. The nature and significance of the breakpoints will become more certain.

The (wing + canard) total C_L is almost invariant with canard setting angle. The Lift curve slopes, theory and experiment, compare well. The C_L offset is possibly due to the Fuselage and Rear strake contributions not yet modelled. The dC_m/dC_L canard contribution is large (unstable) and invariant with canard setting angle. Canard setting angle induces a C_m offset to both the canard and the wing. The wing contribution is relatively stable. With the canard at 0^o, $C_m \sim C_L$ variation for the canard plus wing configuration compares well with experiment over the limited attached flow range ($0.0 < C_L < 0.2$). Chordwise pressure distributions ($C_P - x$ and $C_P - x/c$) are shown in **Fig.13** at $\alpha = 10^o$. Note the amelioration of high LE suctions over the outer wing with twist and camber.

The effect of relaxing the lifting surfaces trailing wakes has also been considered. The canard and wing relaxed wakes at $\alpha = 10^o$, Mach 0.176 are shown in **Fig.14**. "Rolling up" of the tip vortices is evident. The strong influence of the wing on the canard wake can be seen. The effect on total loads is not noticeable. However, the effects of wake relaxation on the wing spanwise loadings at $\alpha = 10^o$ can be seen in **Fig.15**.

4. LONGITUDINAL STABILITY, WING + CANARD + FUSELAGE

Lift and Pitching Moment Comparisons and Stability Derivatives (Reference Condition, Canard $\theta = 0^o$)

For the complete layout of **Fig.9,** the inclusion of fin and body strakes has made a noticeable contribution to C_m and are therefore included in all subsequent evaluations.

Fig.16 shows the relaxed wakes at $\alpha = 10^o$. We note the canard wake lying close to the fuselage side and the obvious effect the wing upper surface pressure distribution has on its streamwise development. **Fig.17** shows the spanwise loadings at $\alpha = 10^o$. Again, we can see the increased inboard wing loading due to relaxation of the wakes. **Figs.18-19** shows the effect of relaxed wakes on wing chordwise C_P distributions ($C_P - x$ and $C_P - x/c$) at $\alpha = 10^o$. Increased LE suctions are evident over the inner wing together with a corresponding reduction in LE suction over the outer wing. The overall effect is an increase in C_L from 0.468 to 0.490. Wake relaxation effects are included in the majority of analysis.

Fig.20 shows a matrix of relaxed wake geometry covering a range of $\alpha = 0^o, 5^o, 10^o, 15^o, 20^o$ for sideslip = $0^o, 5^o, 10^o$. For the symmetric cases ($\beta = 0^o$), flow remains symmetrical about the centerline ($y = 0$) as α increases.

Fig.21 shows the C_L and C_m comparisons with experiment and other CFD codes. Note the excellent agreement with the CFD results and lift forces from experiment. There are a series of discontinuities in the experimental C_m curve that are not reproduced either by the present predictions or the CFD. Nevertheless, there is a region where the trends are nearly linear. Possible reasons for the breakpoints in the C_L and C_m trends were noted on **Fig.12**. This type of analysis is extremely important when evaluating performance. The nature and significance of the breakpoints will become more certain as work progresses.

Over the "linear" ranges, we can now compare the various lift and Cm curve offsets and slopes, thus yielding the primary set of longitudinal stability derivatives.

	Experiment	**Panel Code**	**CFD**
$C_L(\alpha = 0)$	–0.0770	–0.0348	–0.040
$\alpha(C_L = 0)$	1.68	0.658	0.0833
$dC_L/d\alpha$	0.048	0.0529	0.048
$C_m(\alpha = 0)$	–0.0092	–0.0091	–0.0031
$C_m(C_L = 0)$	–0.0062	–0.0076	–0.0011
$dC_m/d\alpha$	0.0020	0.0023	0.0023
dC_m/dC_L	0.041	0.044	0.048

It must be remembered that the panel code is run in inviscid mode and this will naturally predict slightly higher lift curve slopes than experiment and Navier Stokes CFD. This is considered encouraging and further work with thin boundary layers could be anticipated.

Drag Comparisons

The Drag analysis follows from **Figs.22 & 23**. In simplest terms, the C_D trends are best analysed in terms of C_L^2. This yields a curve in three portions with different slopes and two breaks as depicted in **Fig.23**. The attached flow panel code provides the first slope. The $C_L \tan(\alpha)$ curve provides the third slope. The second break point and the second slope follow from attained thrust approaches. See Refs.6-7. For further work on these lines is needed. Additional complexities arise due to canard setting angle.

Effect of Canard Setting Angle ($\theta = 0^o, -5^o, +5^o$) on Lift & Pitching Moment

The effect of canard setting angle has been derived for the Wing and Canard only configuration with rigid wakes. Both $dC_L/d\theta$ and $dC_m/d\theta$ are invariant with α.

	Panel Code
$dC_L/d\theta$	$\tilde{}$ 0.0 (small)
$dC_m/d\theta$	0.007

It is interesting to note that in this fairly close-coupled layout, the lift increment arising on the canard is more or less lost over the wing. So the canard essentially acts as a pitch generator as well as moving the neutral point forward of the wing only neutral point. Positive Canard deflection shifts the neutral point rearwards 0.077% c_{ref} /^{o}. The effect of wake relaxation may also be considered.

Effect of TE Flap Deflection (TEF = 0^o, $+5^o$) on Lift & Pitching Moment

The effect of Wing TE Flap deflection has been derived for the Wing, Canard and Fuselage configuration with rigid wakes. The full-span TEF geometry is defined in **Figs.1 & 6**. The wing root (fuselage side) TE has not been deflected. Wing TE deflected downwards is defined as +ve TEF. The

effect of relaxed wakes at $\alpha = 10^o$ has also been considered. There is slight, non-linear variation in both $dC_L/dTEF$ and $dC_m/dTEF$ as in the following table:

	Panel	α^o	
$dC_L / \delta TEF$	0.0247	0	
$dC_L / \delta TEF$	0.0241	6	
$dC_L / \delta TEF$	0.0233	10	
$dC_L / \delta TEF$	0.0242	10	Relaxed wakes
$dC_m / \delta TEF$	0.00998	0	
$dC_m / \delta TEF$	0.00978	6	
$dC_m / \delta TEF$	0.00952	10	
$dC_m / \delta TEF$	0.00994	10	Relaxed wakes

Relaxing the wakes has an effect on both the dC_L / dTEF and dC_m / dTEF derivatives. Further work is required to establish the most suitable wake geometry at the deflected flap TE.

Effect of LE Flap Deflection (LEF = 0°, +5° Down) on Lift & Pitching Moment

The main purpose of LE flap deflection is to suppress separation / vortex onset and development and hence reduce drag. The LEF geometry is defined in **Figs.1 & 6**. The LEF extends from y/s = 0.36 to the tip. Wing LE deflected downwards is defined as +ve LEF. The effect of LEF deflection has been derived for the Wing, Canard and Fuselage configuration with rigid wakes. The effect of relaxed wakes at $\alpha = 10^o$ has also been considered.

There is slight, non-linear variation in both $dC_L/dLEF$ and $dC_m/dLEF$ as can be seen in the following table.

	Panel Code	α^o	
$dC_L / \delta LEF$	–0.0007	0	
$dC_L / \delta LEF$	–0.0005	6	
$dC_L / \delta LEF$	–0.0005	10	
$dC_L / \delta LEF$	–0.0004	10	Relaxed wakes
$dC_m / \delta LEF$	–0.0002	0	
$dC_m / \delta LEF$	–0.0003	6	
$dC_m / \delta LEF$	–0.0002	10	
$dC_m / \delta LEF$	–0.0003	10	Relaxed wakes

Spanwise C_P distributions from experiment at 66% wing root chord (**Fig.6**) are compared with theory in **Fig.24** for $\alpha = 12^o$, 17^o and 25^o. There is very good agreement over the attached flow range, e.g. $\alpha = 12^o$. Vortical flow and flow breakdown are evident in the experiment at $\alpha = 17^o$ and 25^o respectively.

5. SELECTED DIRECTIONAL STABILITY, WING + CANARD + FUSELAGE

Effect of Sideslip

For the full panelling geometry shown in **Fig.9** we look at typical combinations of sideslip $\beta = 5^o$ & 10^o (positive, nose to right) for $\alpha = 0^o$, 5^o, 10^o, 15^o & 20^o. **Fig.20** shows a matrix of relaxed wake geometries. For the symmetric cases ($\beta = 0^o$), flow remains symmetrical about the centerline (y = 0) as incidence increases. At $\beta = 5^o$, the left canard wake lies to the left of the fin as incidence increases up to $\alpha = 15^o$. At $\alpha = 20^o$, the left canard wake bifurcates, part of the wake passing over the top and to the right of the fin. At $\beta = 10^o$, $\alpha = 0^o$ & 5^o part of the left canard wake passes to the right of the fin, the major part remaining to the left. As incidence increases further, the entire left canard wake passes over the LE of the fin to the right side. There is little canard wake effect on the left wing and the right canard wake clearly affects the right inner wing.

Fig.25 shows spanwise load distributions (C_{LL}, $C_{LLc/cave}$, $C_{DLc/cave}$ and $C_{mLc/cave}$) for the Canard and Wing with relaxed wakes, through $\alpha = 10^o$, 15^o and 20^o for $\beta = 0^o$, 5^o and 10^o. The asymmetrical nature of the distributions is evident at $\beta = 5^o$ and 10^o. Wing chordwise Cp distributions at corresponding sideslip and incidence are shown in **Fig.26**. The symmetric case Cp distributions are established at $\beta = 0^o$, the effect of sideslip on the LE suctions is then evident. At $\beta = 10^o$, the left wing LE suctions are markedly reduced (reduced sweep, higher AR) with the converse occurring on the right wing. The "zones of influence" of the relaxed canard wakes on the lateral force and moment coefficients are noted in **Fig.27**. The effect of wake relaxation on the variation of C_l with C_L at $\beta = 10^o$ is highlighted in **Fig.27(c)**. Without relaxed wake, the variation is linear. With wake relaxation, the influences of the left canard wake passing over the fin and of the right canard wake on the right wing on C_l are evident.

At $\alpha = 0$, derivatives arising from $0 < \beta < 5$ are

	Panel Code	
$dC_Y / d\beta$	0.01653	Side Force
$dC_l / d\beta$	-0.00036	Rolling Moment
$dC_n / d\beta$	0.00068	Yawing Moment
dCL / dβ	0.00044	Lift
dCm / dβ	-0.00068	Pitching Moment

6. LONGITUDINAL TRIMMING ASPECTS

With the various longitudinal control powers available, the trimmed behaviour can be derived at different C_L levels. **Fig.28** shows the predicted $C_m - C_L$ behaviour with different canard settings. **Fig.29** relates the canard setting θ and TEF δF schedule for different stability levels. We assume that for neutral stability, the canard has near zero load. Positive canard setting θ corresponds to stable static margin and vice-versa. A recent comparison set of results (different methods) on longitudinal characteristics (canard 0 setting) is shown in **Fig.30**, Ref.8. Note that the experimental trends of Cm are not reflected by any method. So a realistic canard setting must be considered for comparisons at high AoA.

7. CONCLUDING REMARKS & GENERAL INFERENCES

This paper is via the initiative of the NATO RTO-AVT-161 Task Group. The group is aimed at the assessment of Stability and Control Prediction Methods for the NATO Air and Sea Vehicles (essentially complex configurations). The assessments need to include the absolute values of forces and moments as well as the various symmetric and asymmetric stability derivatives, both steady and unsteady. This paper relates to analysis of the canard-delta X-31 "Vector" aircraft.

Low speed experimental data is available on an X-31 model tested by DLR. The main focus of the paper has been in the use of linear theory and Surface Singularity methods (Panel codes). Results have been compared with experiment and other CFD methods. The main emphasis has been on longitudinal stability aspects with component contributions. However, selected asymmetric effects have also been considered.

For the symmetric cases, the predictions have shown good agreement for lift with experiment and CFD up to α about 15^o. For pitching moment, agreement with other

CFD results is good up to α of 15°. The experiments show a more discontinuous behaviour beyond α about 10°.

In real trimmed flight, as aircraft angle of attack or C_L increases, canard angle will reduce and TEF will deflect upwards. An example of trimming has been given.

For the asymmetric cases with sideslip, a limited set of stability derivatives have been obtained. These look reasonable but need to be compared with experiments.

Work is needed for estimation of roll / yaw derivatives.

The work so far has been interesting and encouraging. It has led to an improved understanding of the complex configurations with strongly interacting and separating / vortical flows. It is remarkable that low-order theories apply reasonably well to α of 15° or so, with results being competent with high-order CFD solvers.

We have shown that a considerable portion of the overall assessment (stability and control) of a complex configuration can be achieved rapidly using panel methods. Viscous effects can be introduced, establishing possible flow-break onsets requiring further investigation. This allows more costly high order methods and wind tunnel testing to be focussed on key areas. Configuration refinements can be introduced where necessary before very costly model manufacture is undertaken.

In the wider future perspective, an understanding has evolved for either exploitation or avoidance of the complex flows. This has been an important motivation.

ACKNOWLEDGEMENTS

This work is part of current in-house R & D activities. No external financial support has been received. Nevertheless it has been a sizeable undertaking, all in the cause of science! The authors have pleasure in acknowledging work of DNW in supplying Wind Tunnel results and helpful discussions with Dipl. -ing. Andreas Schuette. Any opinions expressed are those of the author. The author has been privileged to be a member of AVT-161 task group. It is felt that the Task group work has been truly inspirational and thorough, being accomplished by motivated and expert researchers. Opportunities for future collaboration are warmly invited.

REFERENCES

1. SCHUETTEe, A.; CUMMINGS, M.; LOESER, T.; VICROY, D., “Integrated Computational/Experimental Approach to UCAV and Delta-Canard Configurations Regarding Stability & Control”. 4th Symposium on Integrating CFD and Experiments in Aerodynamics, 2009.

2.NANGIA, R.K. & PALMER, M.E., "Application of Subsonic First-Order Methods for Prediction of Inlet & Nozzle Aerodynamic Interactions with Airframe", Symposium on "Aerodynamic Engine/Airframe Integration for High Performance Aircraft & Missiles", Fort Worth, Texas, USA, AGARD CP-498, 1991.

3.NANGIA, R. K., "Low Speed Performance Optimisation of Advanced Supersonic Civil Transport with Different LE & TE Devices", EAC'94, Toulouse, France, October 1994.

4.NANGIA, R.K. & MILLER, A.S., "Vortex Flow Dilemmas & Control on Wing Planforms for High Speeds", Paper Presented at RTO - AVT Symposium, Loen, Norway, May 2001.

5.Report for AVT-161 Task Group.

6.NANGIA, R.K., "Semi-Empirical Prediction of the Vortex Formation on the VFE-2 Configuration (65 deg. Delta Wings with different Leading Edge shapes)”, Chapter 33, RTO-AVT-113 Report, Formal Publication 2008.

7. NANGIA, R.K., "Semi-Empirical Prediction of the Vortex Onset & Progression on 65 deg. Delta Wings (RTO-AVT-113, VFE-2 Facet) ”, 46th AIAA Aerospace Sciences. Meeting, Reno, AIAA-2008-0384, January 2008.

8. TOMAC, M., RIZZI, A., NANGIA, R., MENDENHALL,M.R. & PERKINS, S.C., ” Comparing & Benchmarking Engineering Methods on the Prediction of X-31”, AIAA-2010-4694.

NOMENCLATURE

AR	Aspect Ratio
b	= 2 s, Wing span
c	Local Wing Chord
c_{av}	= S/b, Mean Geometric Chord
c_{aero}	= c_{ref} = Mean Aerodynamic Chord of Wing
C_A	= Axial force/(q S), Axial Force Coefficient
C_{AL}	Local Axial Force Coefficient
C_D	= Drag Force /(q S), Drag Coefficient (C_{Di}+ C_{D0})
C_{Di}	Lift Induced Drag Coefficient
C_{DL}	Local Drag Coefficient
CG	Centre of Gravity
C_l	= Rolling Moment/(qSs), Rolling Moment Coefficient
C_L	= Lift Force/(q S), Lift Coefficient
C_{LL}	Local Lift Coefficient
C_m	= m/(q S c_{aero}), Pitching Moment Coefficient
C_{mL}	Local Pitching Moment Coefficient
C_n	= Yawing moment/(q S s), Yaw Moment Coeff.
C_P	Coefficient of Pressure
C_Y	= Side Force/(qS) ,Side-force Coefficient
ΔC_D	Difference in C_D
LE, TE	Leading Edge, Trailing Edge
LEF, TEF	Leading Edge Flap, Trailing Edge Flap
L/D	Lift to Drag ratio
m	Pitching moment
M	Mach Number
q	= 0.5 ρ V^2, Dynamic Pressure
Re	Reynolds Number, based on c_{aero}
s, S	semi-span, Wing Area
Sc	Canard Wing Area
S	Main Wing Area, also Reference
V	Free-stream Velocity
x, y, z	Axes system of an aircraft
x_{AC}	Chordwise position of Aerodynamic Centre
x_{CP}	Chordwise location of Centre of Pressure
y_{CP}	Spanwise location of Centre of Pressure
α	AoA, Angle of Attack
ß	Sideslip Angle
ß	$\sqrt{(1-M^2)}$
λ	Taper Ratio, c_t/c_r
Λ	LE Sweep Angle
η	= y/s, Non-dimensional spanwise distance
ρ	Air Density
δF	TE Flap Deflection
δL	LE Flap Deflection
θ	Canard Setting Angle

Table 1 X-31 VECTOR CONFIGURATION MODEL, DIMENSIONS & DEFINITIONS

		Model Metric Units		Non-Dimensional Units Wing Semi-span = 1.0
Wing Semi-span s		0.5	m	1.0
Wing Span b		1.0	m	2.0
Length with Vector Panel		1.81	m	
Length without Vector Panel		1.706	m	
Inner Wing Chord		0.7903	m	
Wing Area S		0.3984	m^2	1.5936
Canard Span		0.3634	m	
Canard Area S_C		0.04155	m^2	
Mean Aerodynamic Chord	c_{aero}	0.51818	m	1.03636
Mean Aerodynamic Centre	x_{ac}	0.93766	m	x = 1.875, y = 0.0, z = -0.15

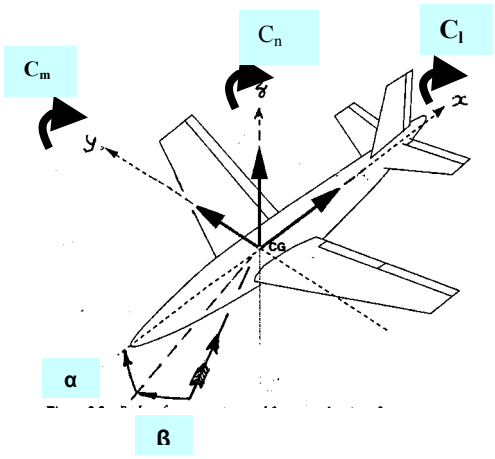

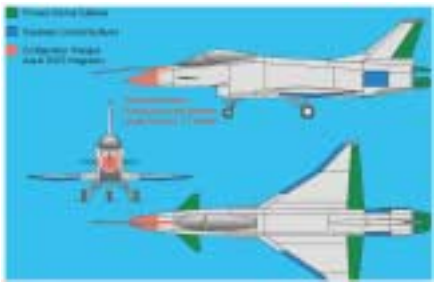

Canards
Inner & Outer LE Flaps
TE Flaps
Rudder

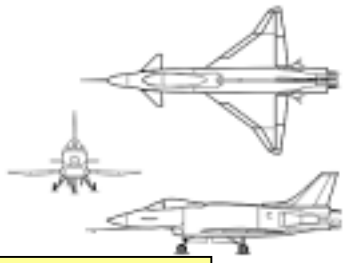

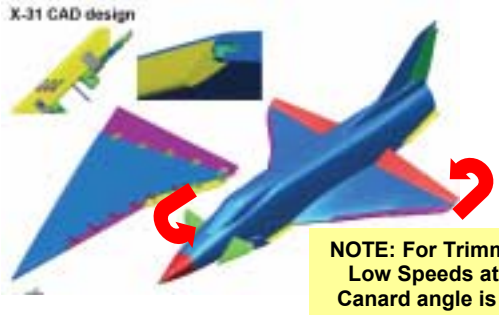

NOTE: For Trimmed Flight at Low Speeds at high AoA, Canard angle is –ve and TE Flap angle is (-ve) up

Fig. 1 X-31 VECTOR CONFIGURATION

Fig. 2 X-31 VECTOR CAD DESIGN - COMPONENTS

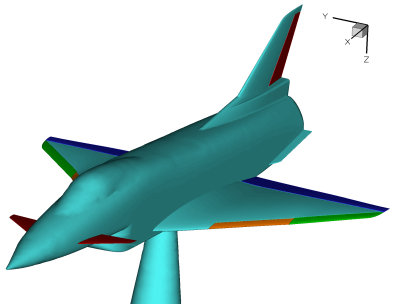

Fig. 3 BELLY STING

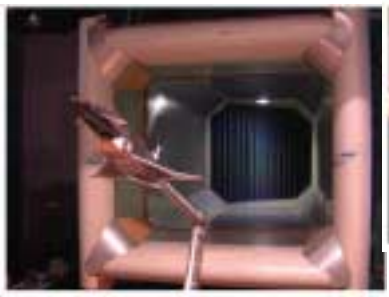

Fig. 4 REMOTE-CONTROL MODEL WITH REAR STING SUPPORT

Occasional Discontinuities in IGES FILES

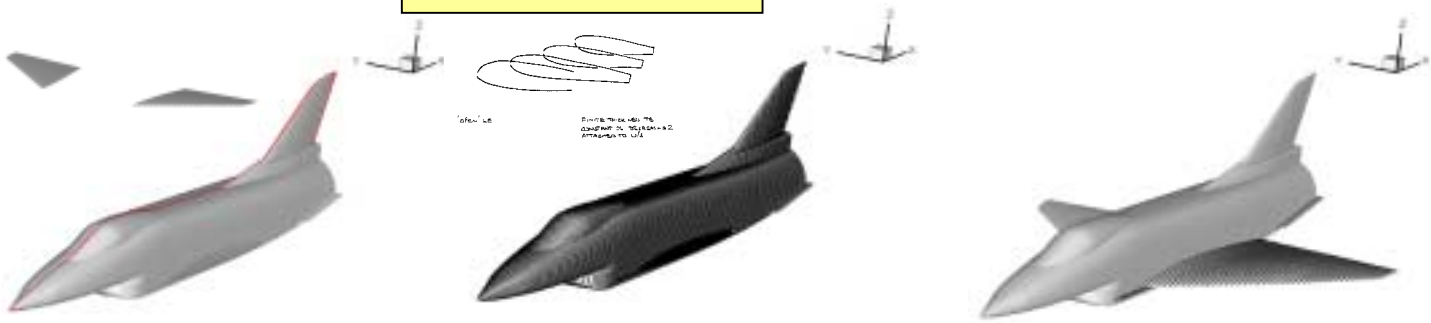

Fig. 5 MODEL GEOMETRY (Cut-Planes) FROM IGES FILES

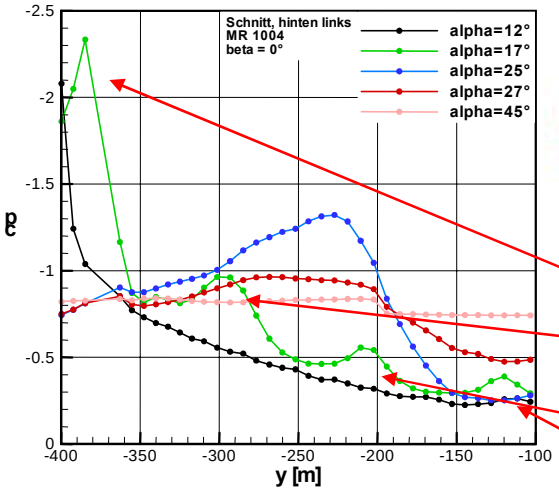

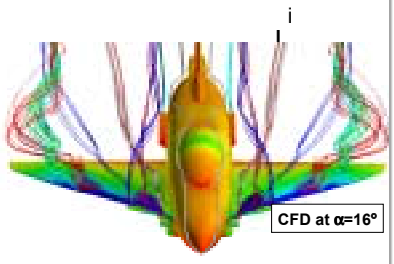

α = 17°:
Outer wing vortex
Outer inner wing vortex (inner LE-flap)
Inner wing vortex
Strake vortex

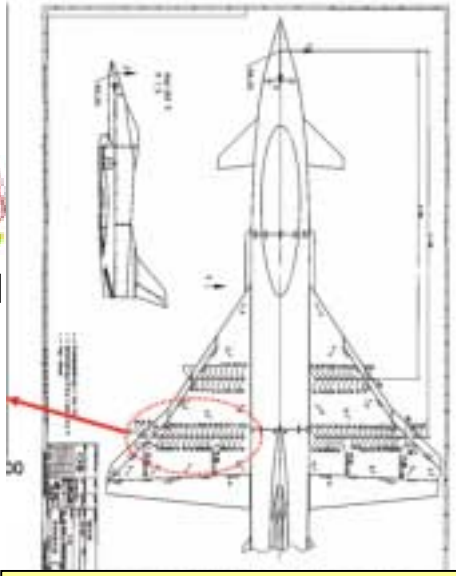

Fig. 6 EXPT., STEADY STATE Cp DISTRIBUTIONS at 70% Cr

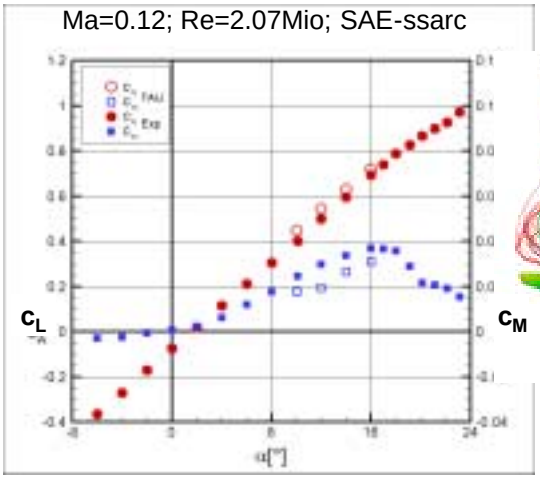

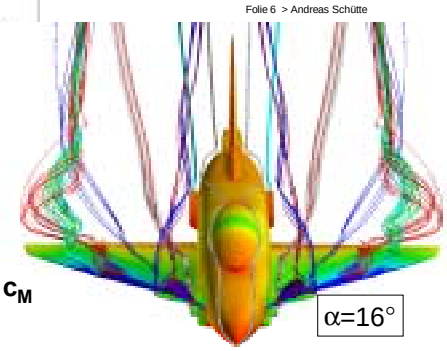

Fig. 7 COMPARISON EXPT & NUMERICAL RESULTS WITH CONTROL DEVICES (Steady State), FULL MODEL WITH FLAPS & STING

Extrapolated Reference Wing & Canard

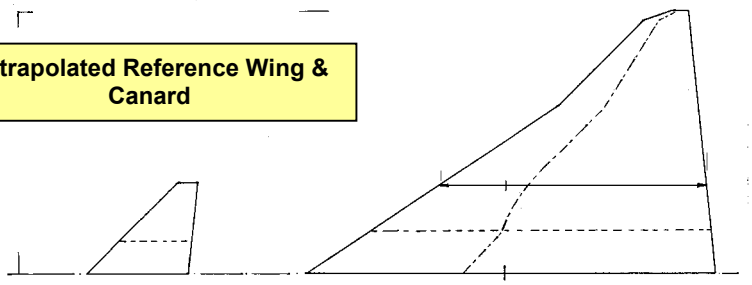

Wing Twist Derived from CATIA

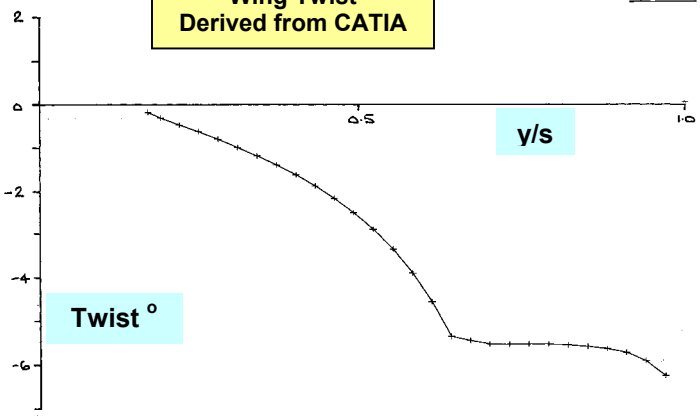

Canard (Planar) t/c = 8% constant

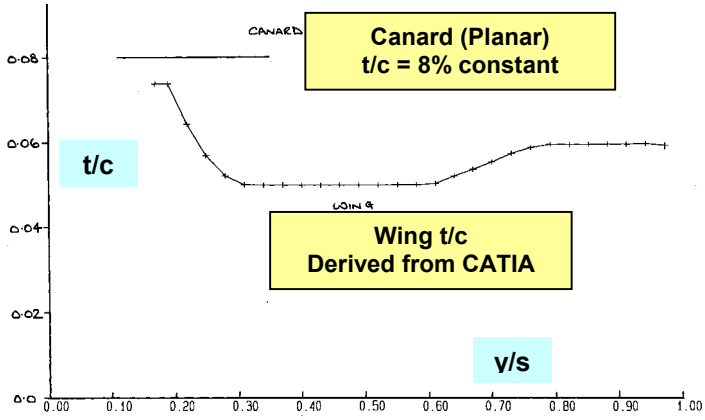

Wing t/c Derived from CATIA

FIG. 8 WING GEOMETRY PARAMETERS

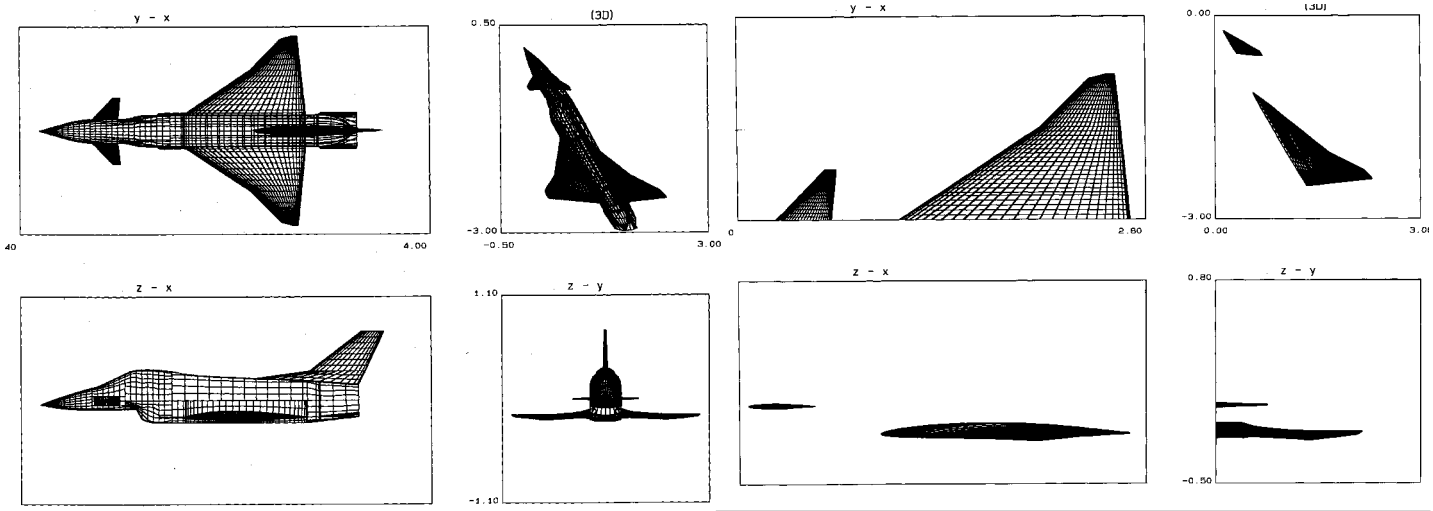

FIG. 9 FULL CONFIGURATION PANELLING

FIG. 10 WING + CANARD ONLY PANELLING, HALF CONFIGURATION, DEVELOPED FROM COMPLETE CONFIGURATION

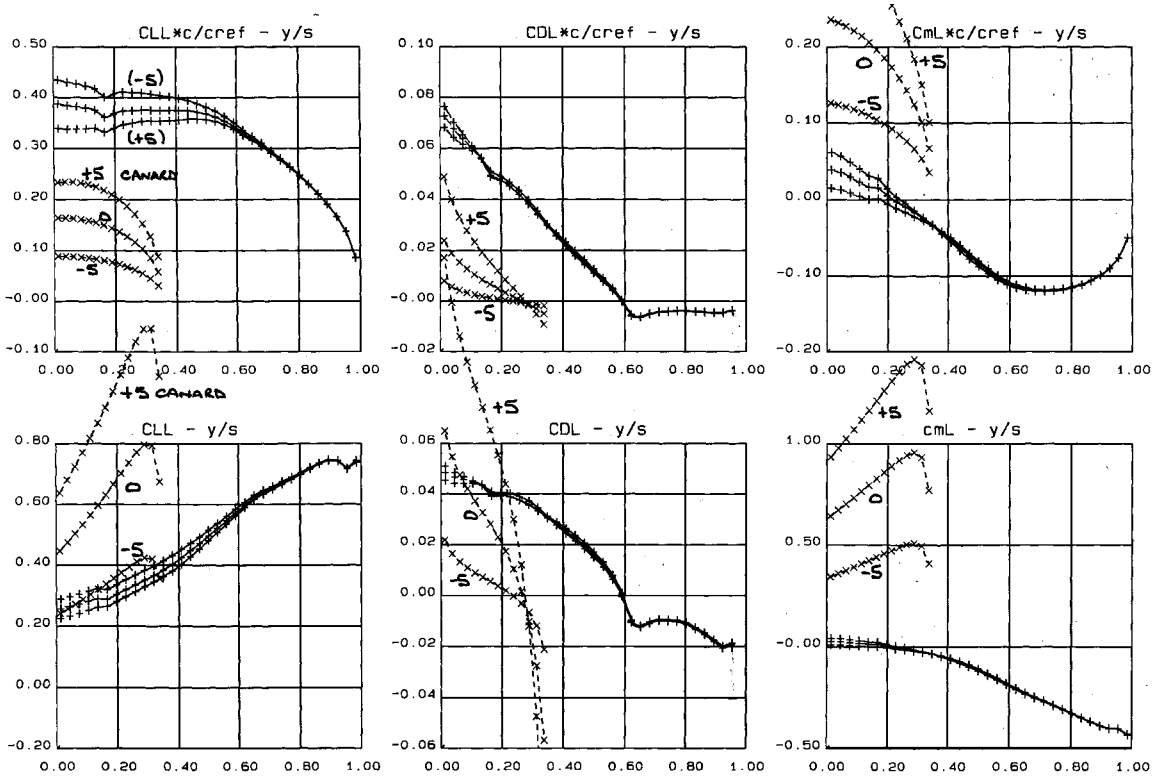

FIG. 11 WING + CANARD ONLY, SPANWISE LOADINGS, EFFECT OF CANARD DEFLECTION, α = 10°

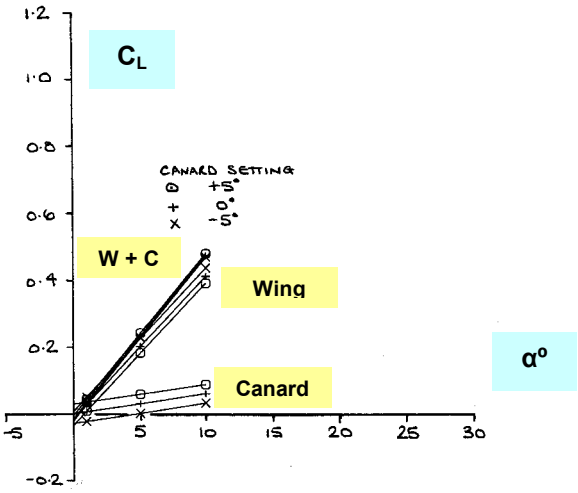

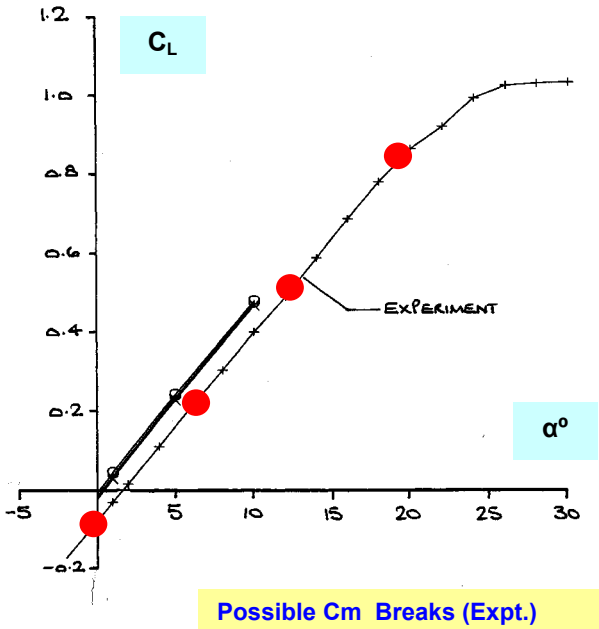

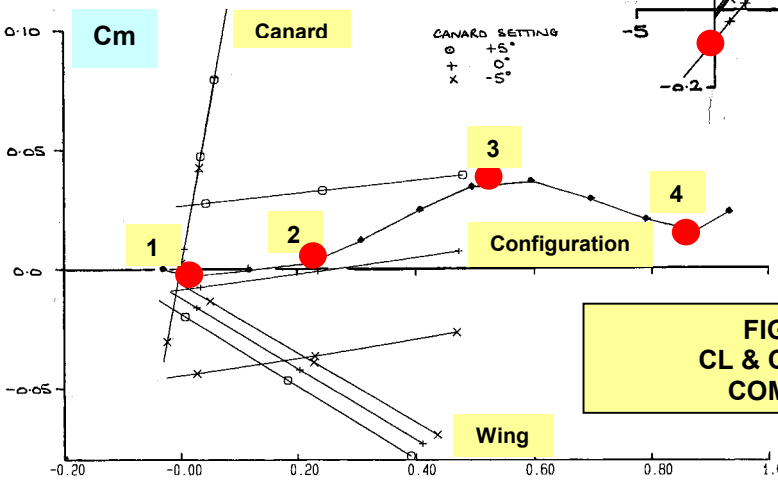

Possible Cm Breaks (Expt.)
1 Wing tip
2 Wing tip & Vortical flow onset
3 canard 'stall'
4 Wing

FIG. 12 WING + CANARD ONLY, CL & Cm COMPONENT BREAKDOWN & COMPARISON WITH EXPERIMENT

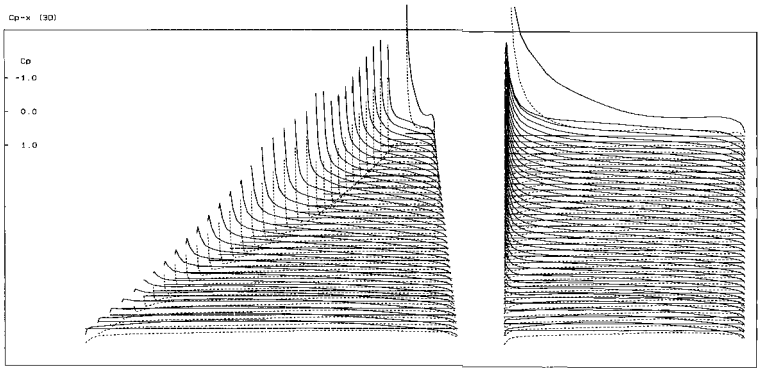

FIG. 13 CHORDWISE Cp DISTRIBUTIONS ON WING, WING + CANARD (0°) ONLY, α = 10° (CL=0.475 (canard 0.061, Wing 0.414)

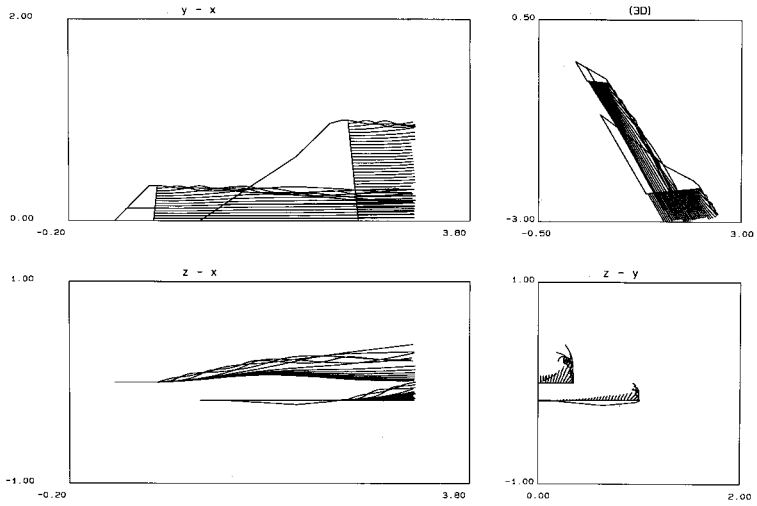

FIG. 14 RELAXED WAKES, WING + CANARD (0°) ONLY, α = 10°

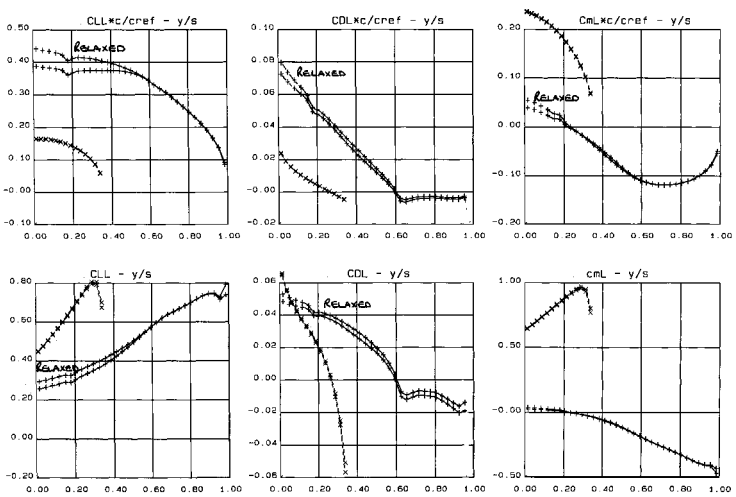

FIG. 15 WING + CANARD (0°), SPANWISE LOADINGS, EFFECT OF RELAXED WAKE AT α = 10°

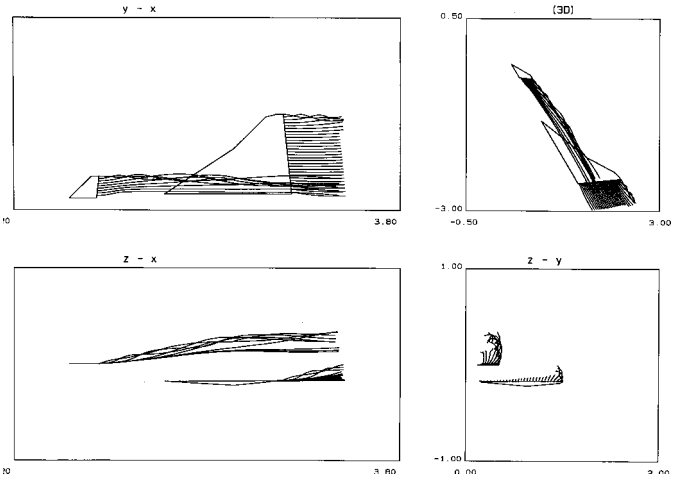

FIG. 16 FULL CONFIGURATION (WING, CANARD (0°) & FUSELAGE), RELAXED WAKES, α = 10°

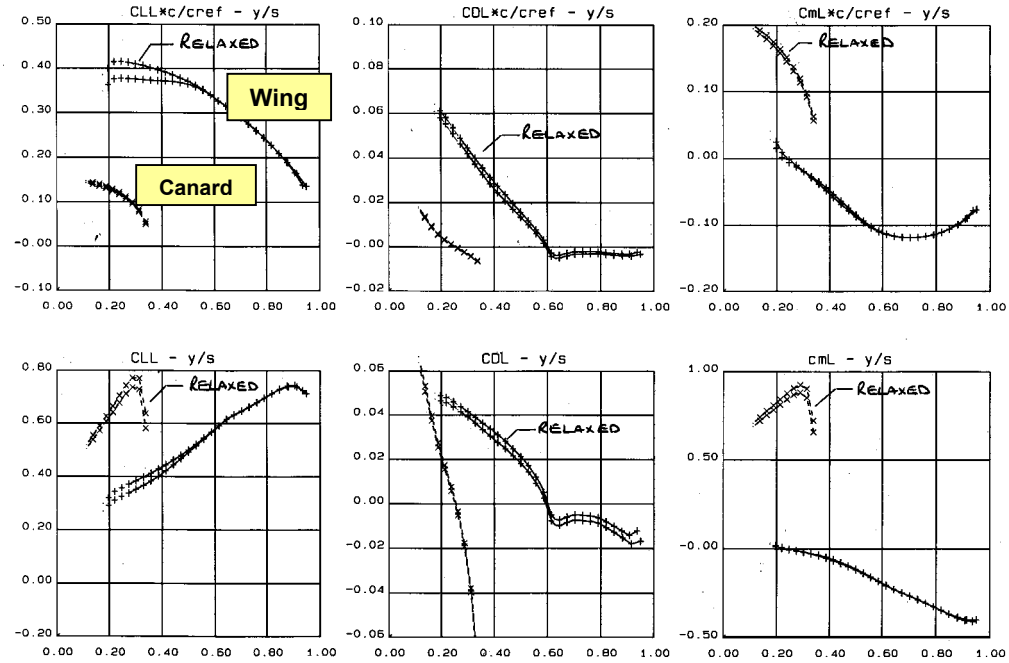

FIG. 17 FULL CONFIGURATION, SPANWISE LOADINGS, α = 10° EFFECT OF RELAXED WAKES

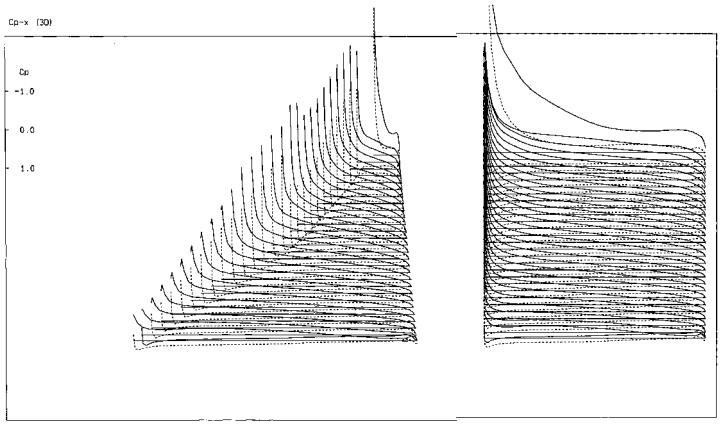

FIG. 18 FULL CONFIGURATION, CHORDWISE Cp DISTRIBUTIONS ON WING, α = 10° RIGID WAKE, CL = 0.467

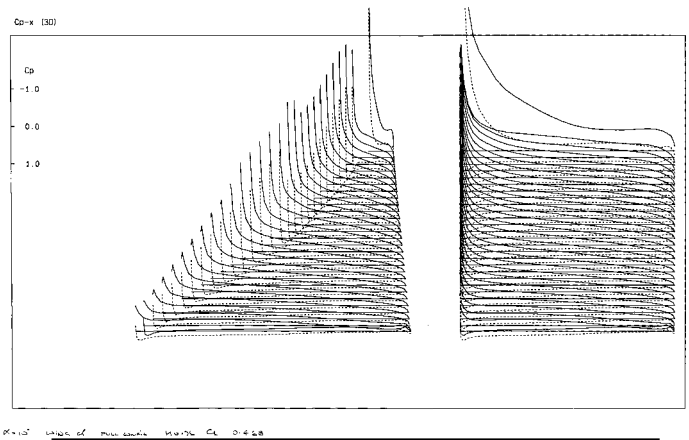

FIG. 19 FULL CONFIGURATION, CHORDWISE Cp DISTRIBUTIONS ON WING, α = 10°, RELAXED WAKE, CL = 0.496

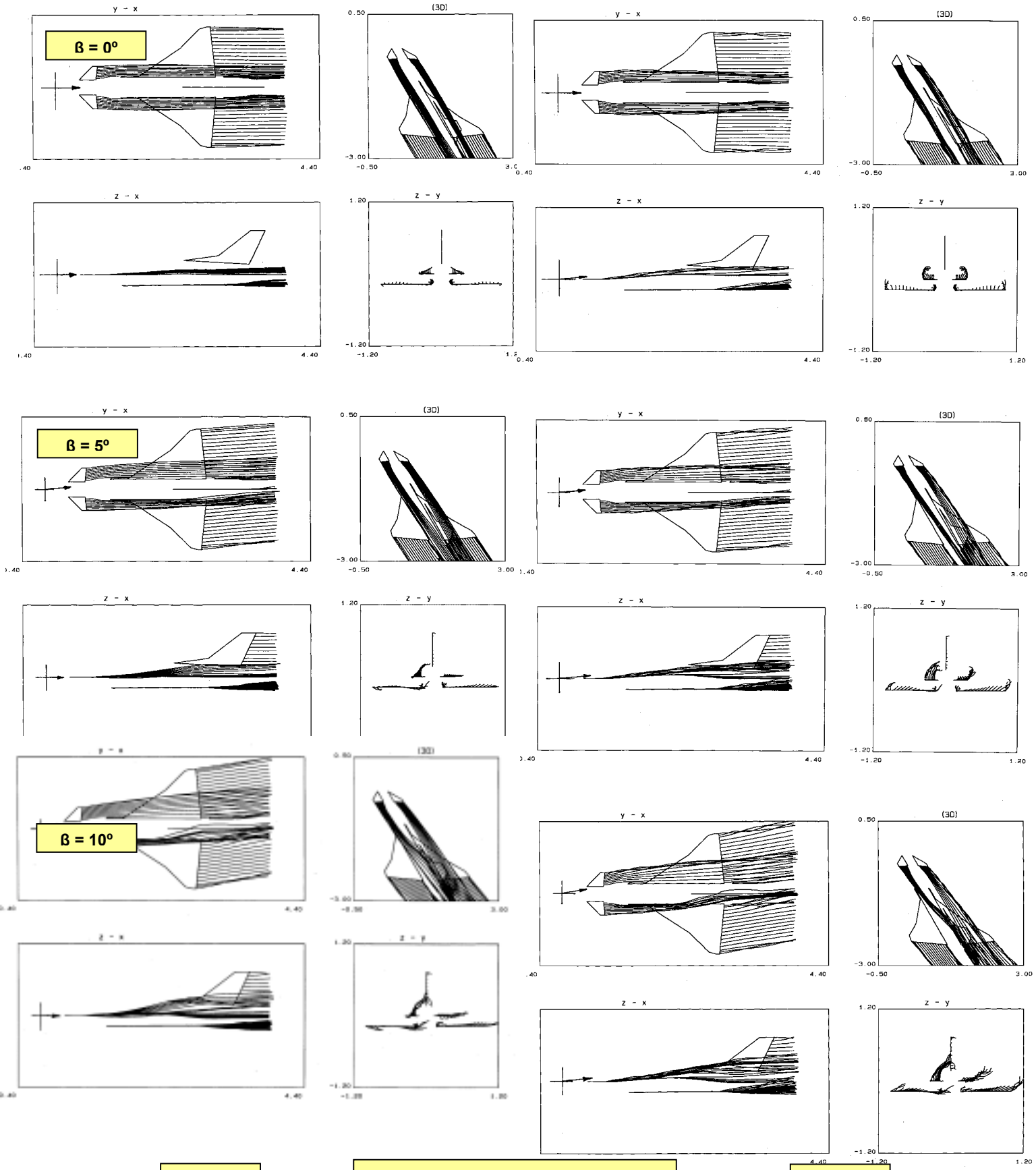

α = 0º

(a) α = 0º & 5º, β = 0º, 5º, 10º

α = 5º

FIG. 20 FULL CONFIGURATION RELAXED WAKES

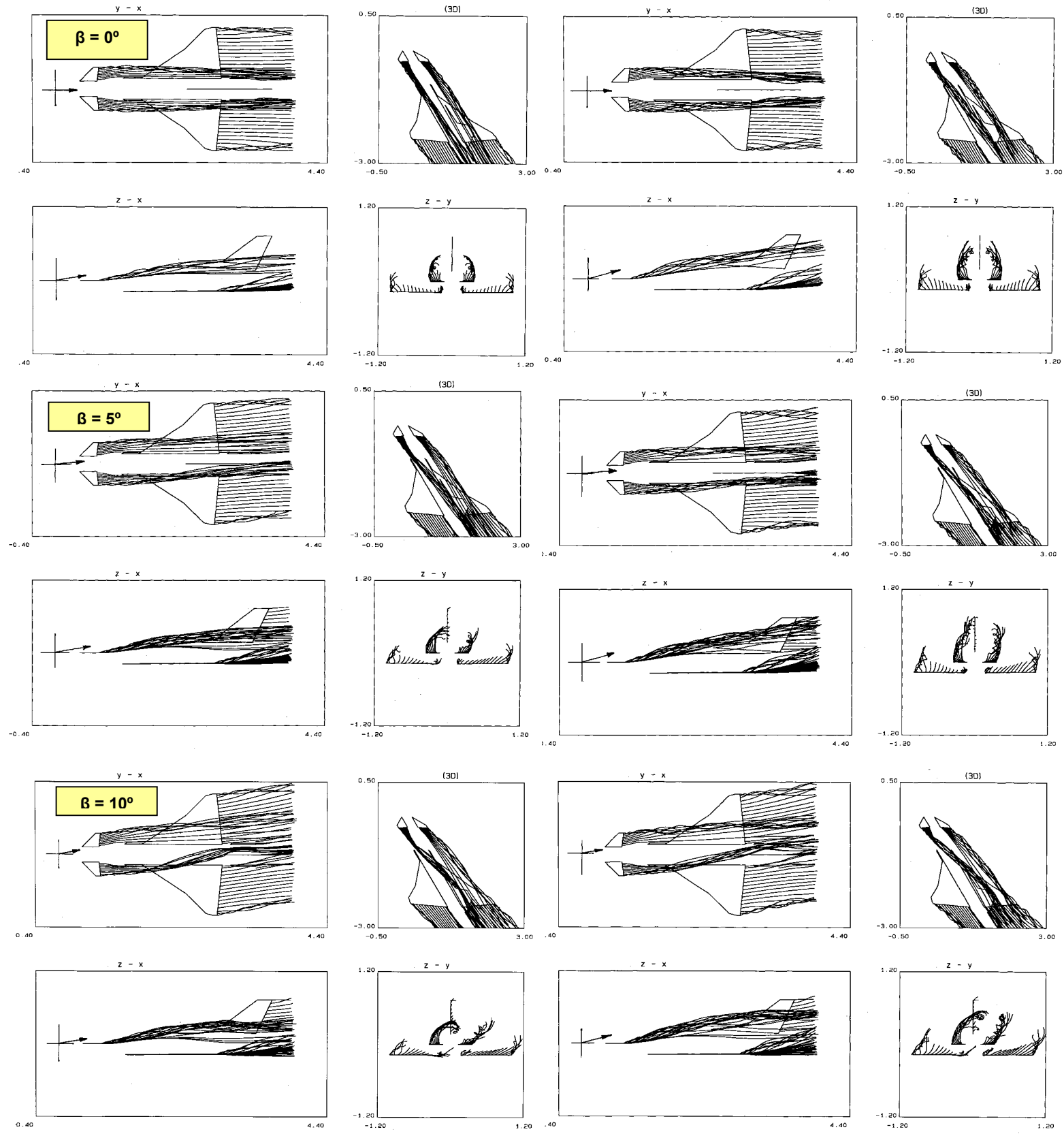

α = 10°

(b) α = 10° & 15°, β = 0°, 5°, 10°

α = 15°

FIG. 20 cont'd

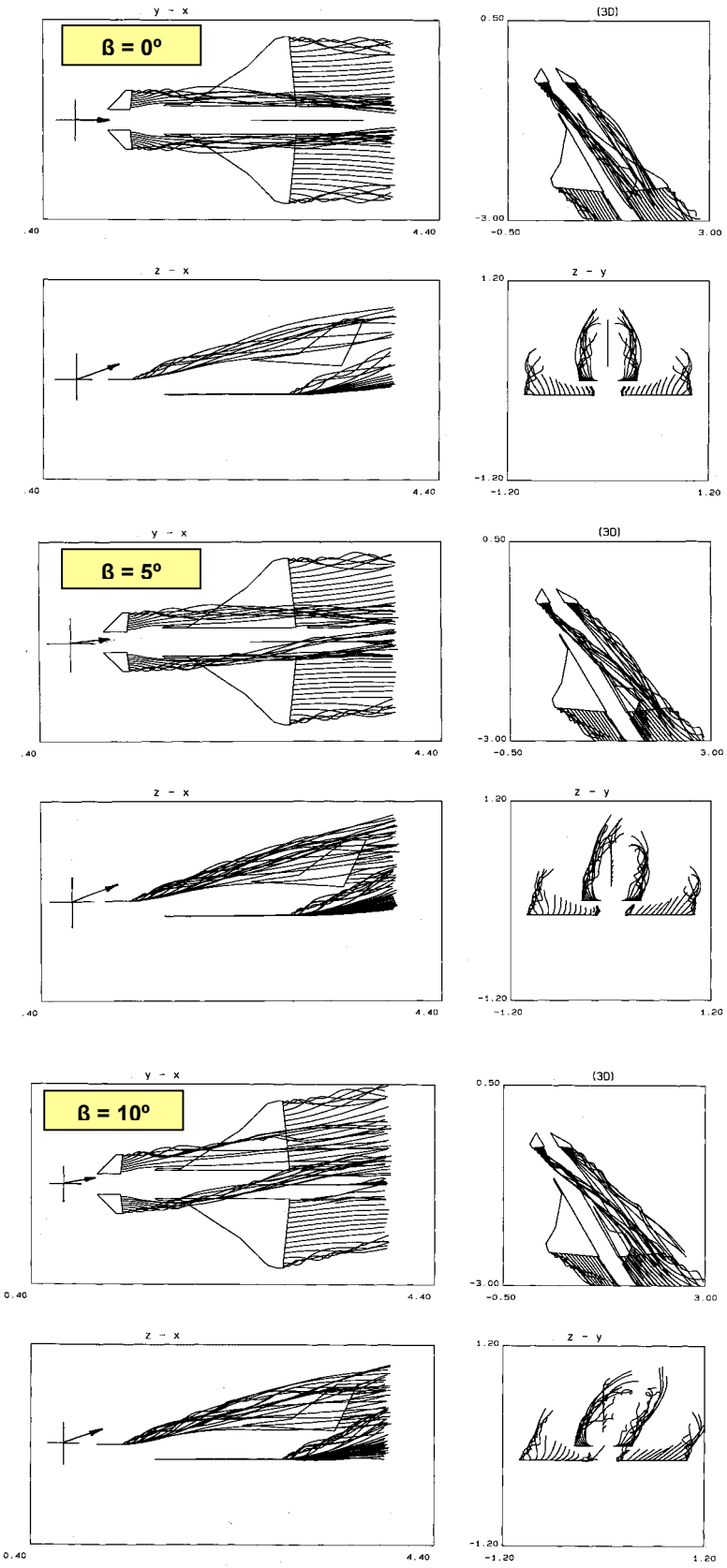

(c) α = 20°, β = 0°, 5°, 10°

FIG. 20 cont'd

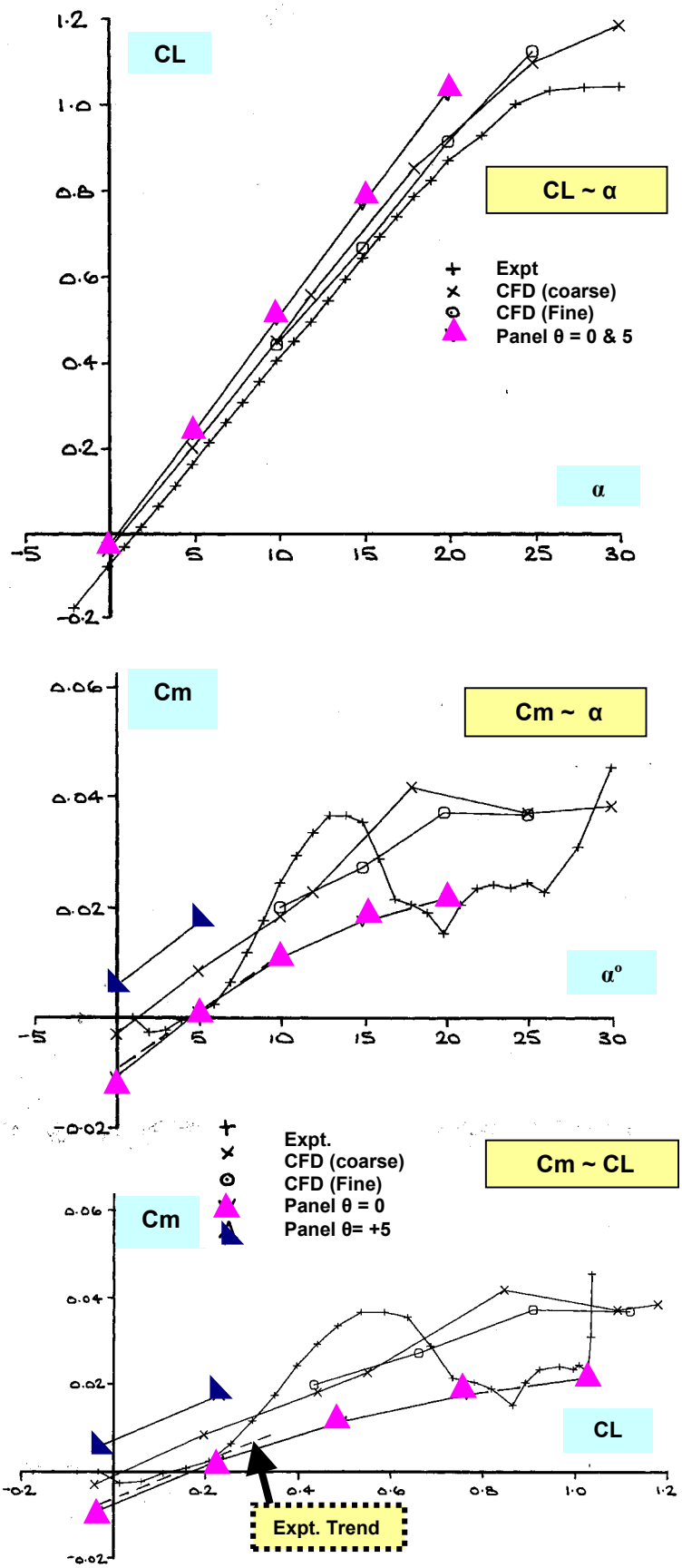

FIG. 21 FULL CONFIGURATION, FORCE & MOMENT COEFFICIENT VARIATIONS

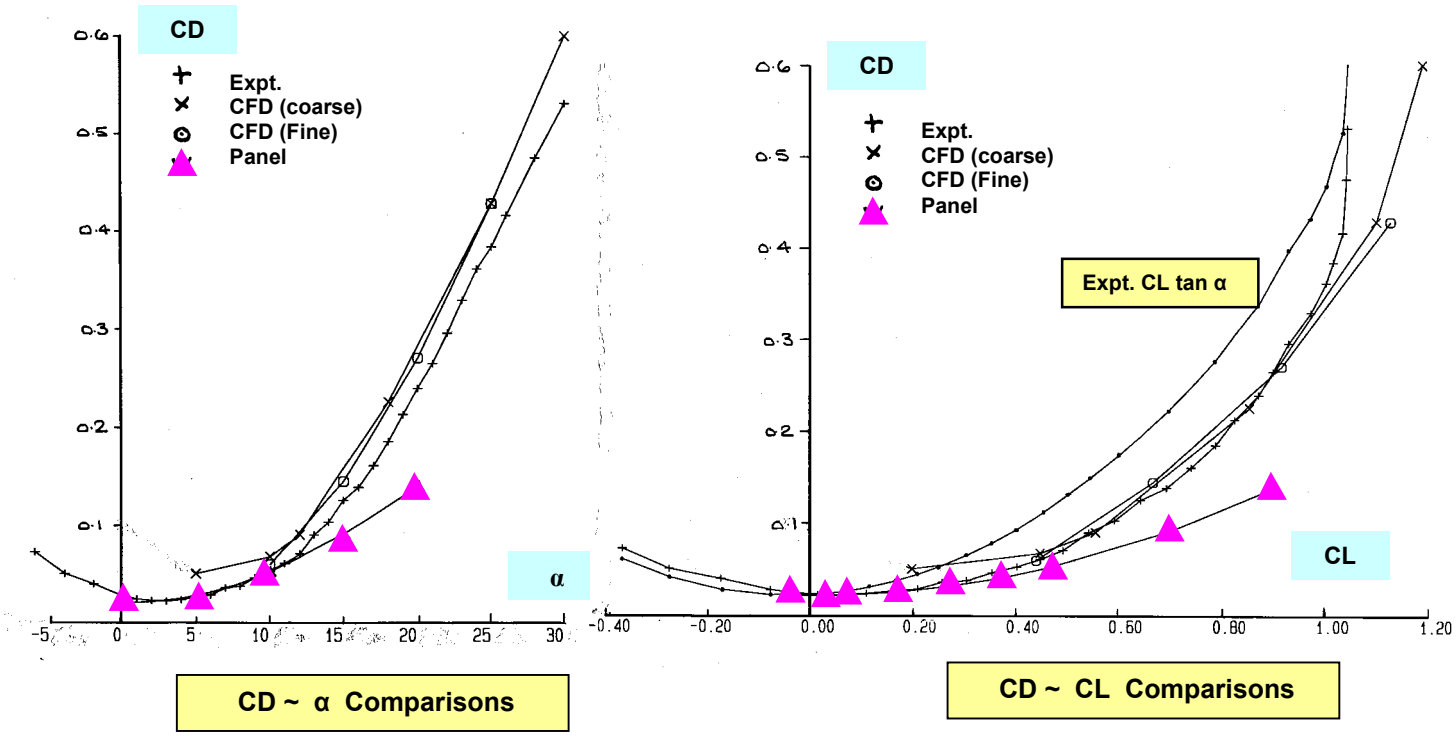

FIG. 22 FULL CONFIGURATION, CD COMPARISONS, RELAXED WAKE

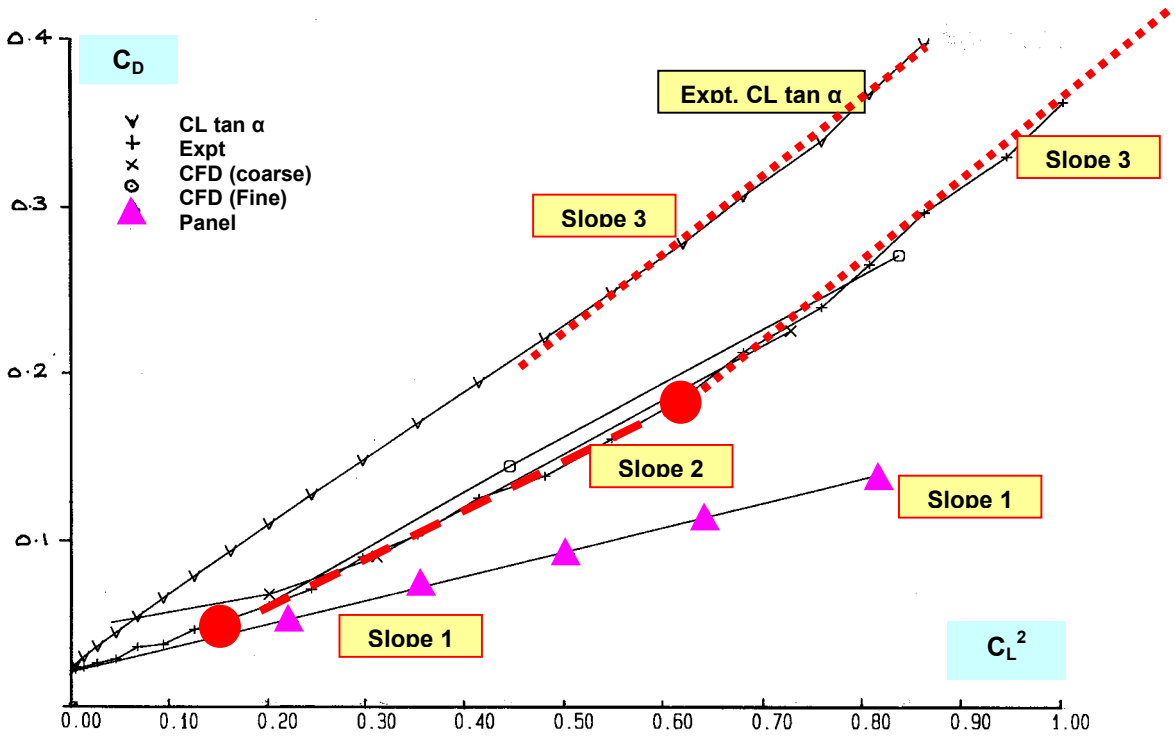

FIG. 23 FULL CONFIGURATION, $C_D \sim C_L^2$ ANALYSIS

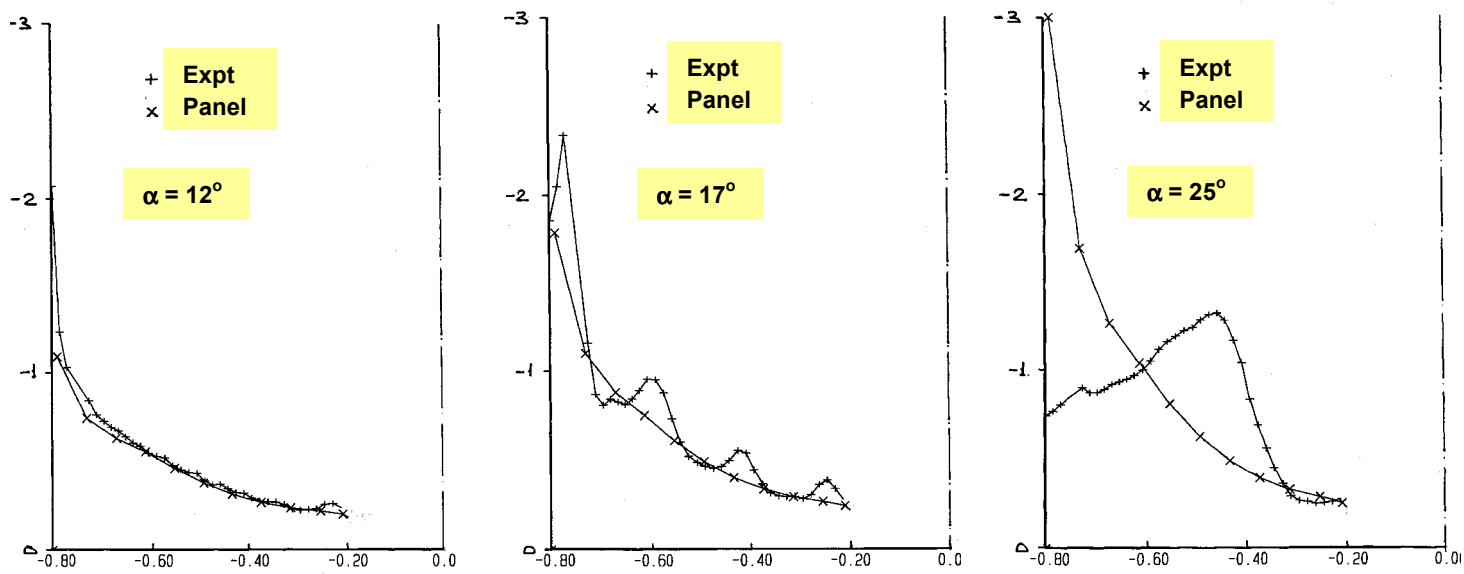

Fig. 24 SPANWISE Cp DISTRIBUTIONS, UPPER SURFACE at α = 12°, 17° & 25°

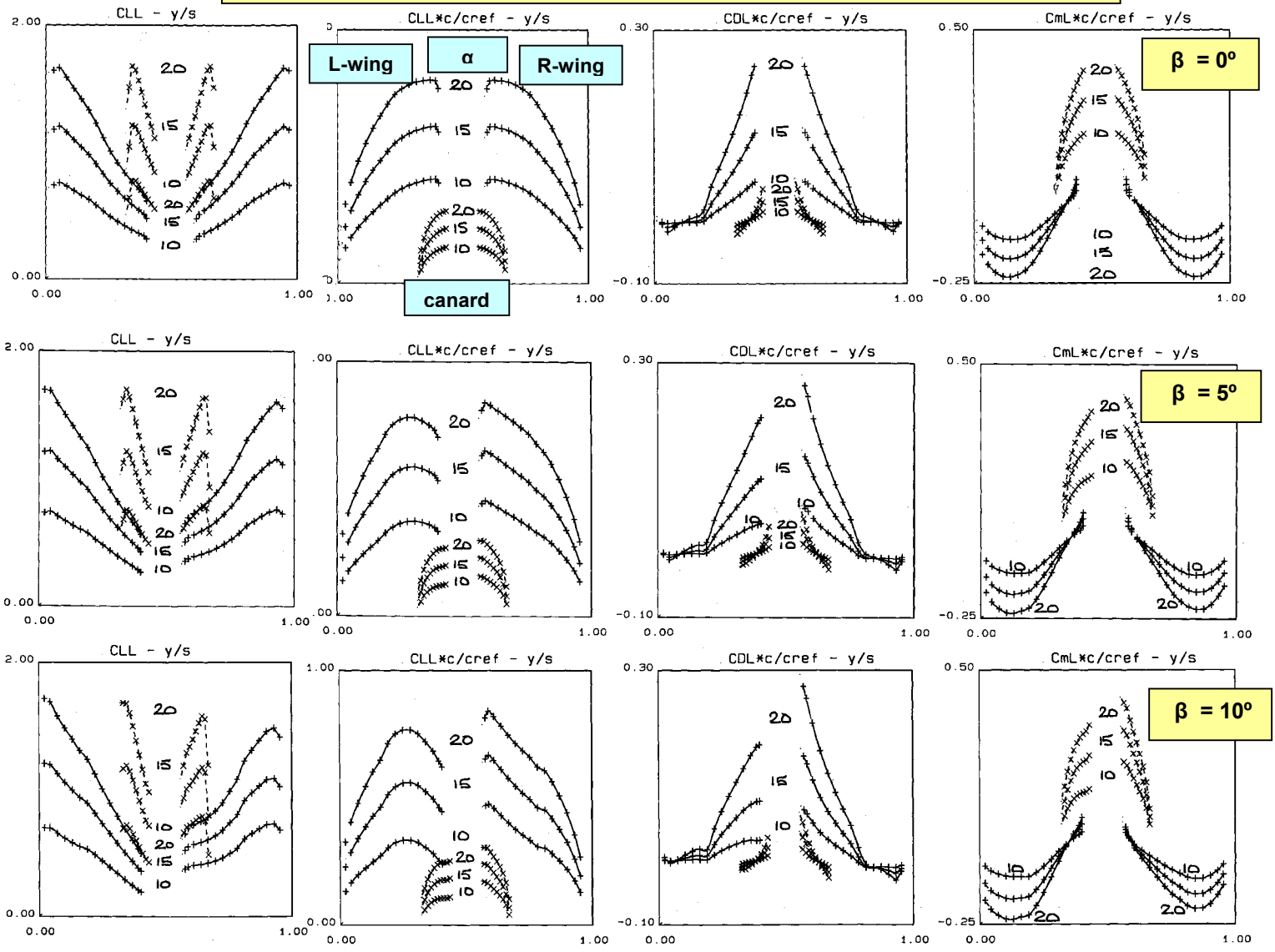

FIG. 25 FULL CONFIGURATION SPANWISE LOADINGS, α = 10°, 15° & 20°, β = 0°, 5°, 10°

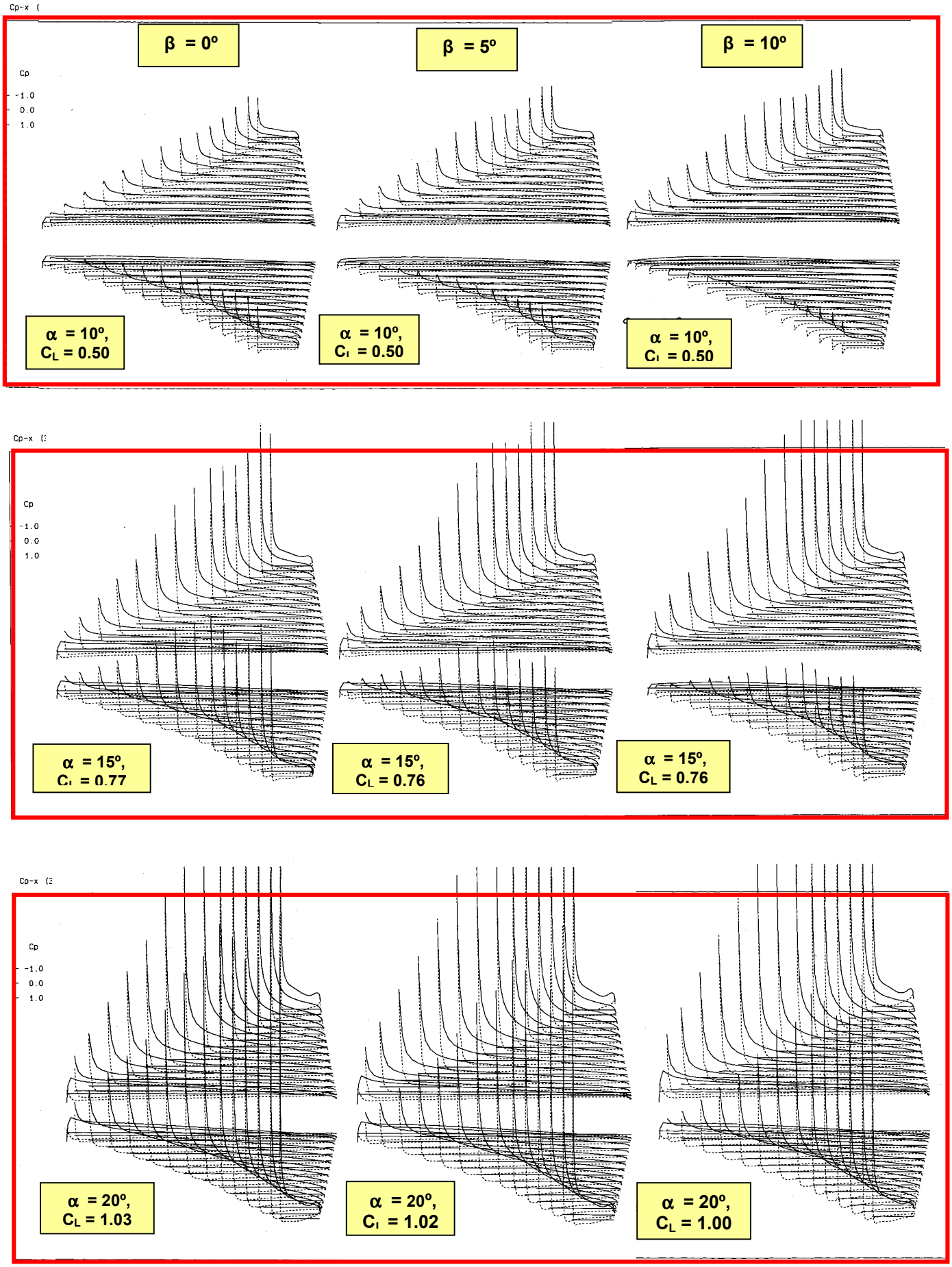

Fig. 26 CHORDWISE Cp DISTRIBUTIONS ON WING, FULL CONFIGURATION

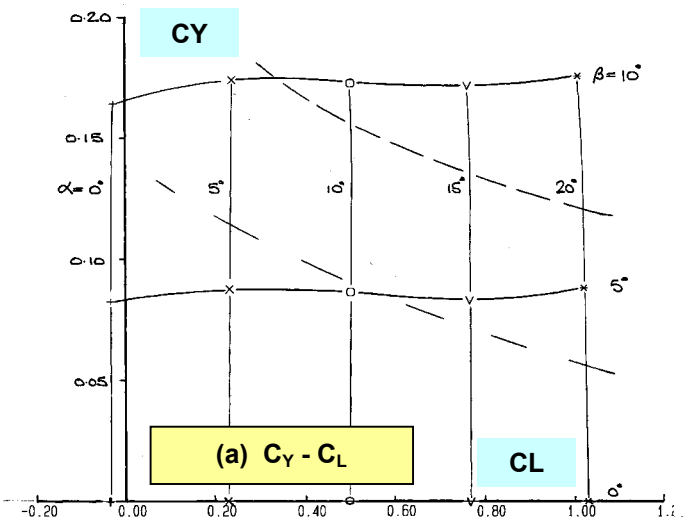

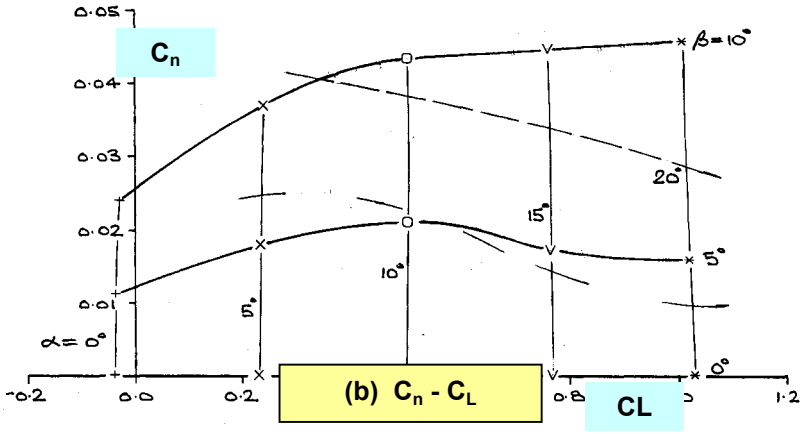

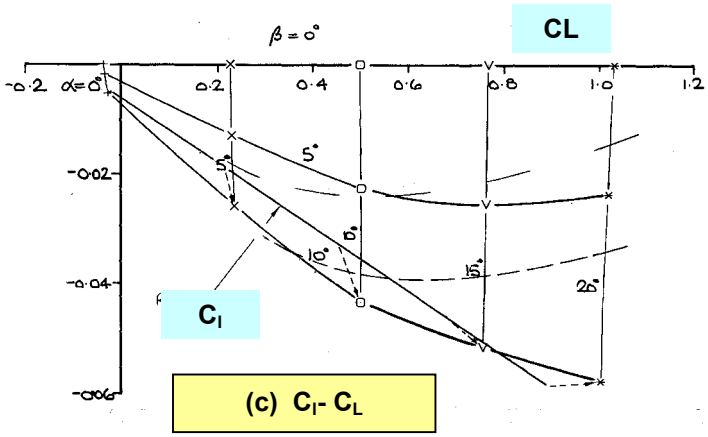

As C_L and β increase
Left Canard wake bifurcates
Left Canard wake lies to right of Fin

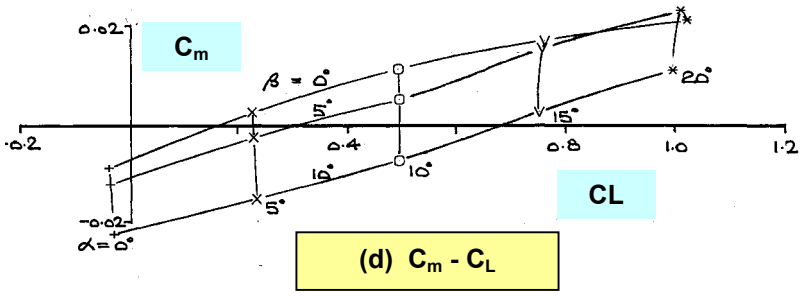

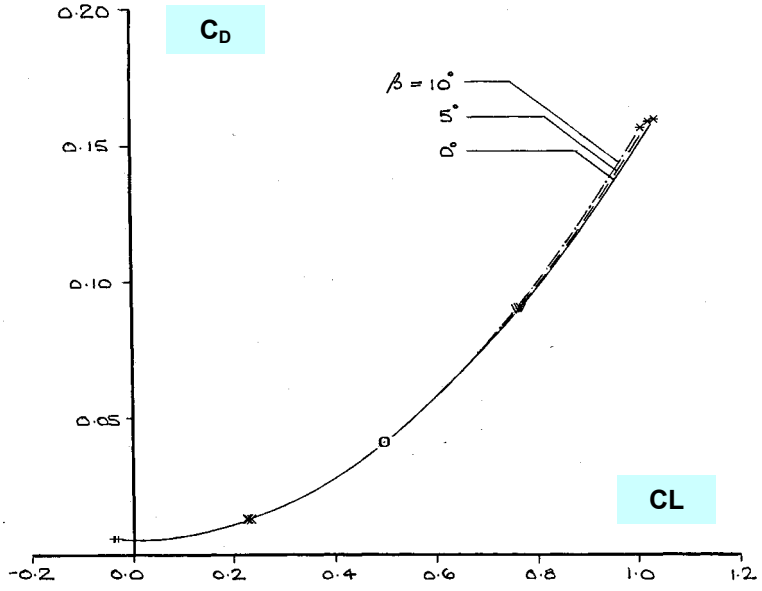

Fig. 27 FULL CONFIGURATION, SIDESLIP EFFECTS, FORCE & MOMENT COEFFICIENT VARIATION WITH C_L

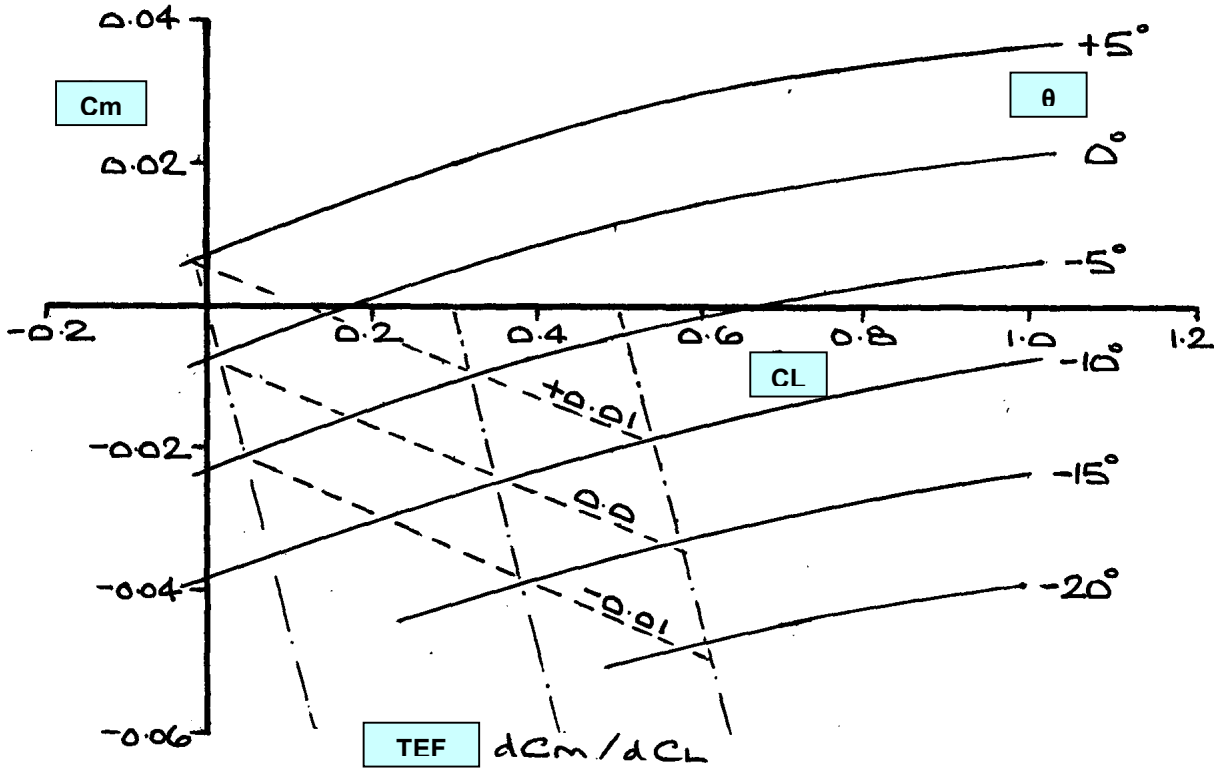

FIG. 28 FULL CONFIGURATION, Cm ~ CL WITH CANARD SETTING EFFECTS

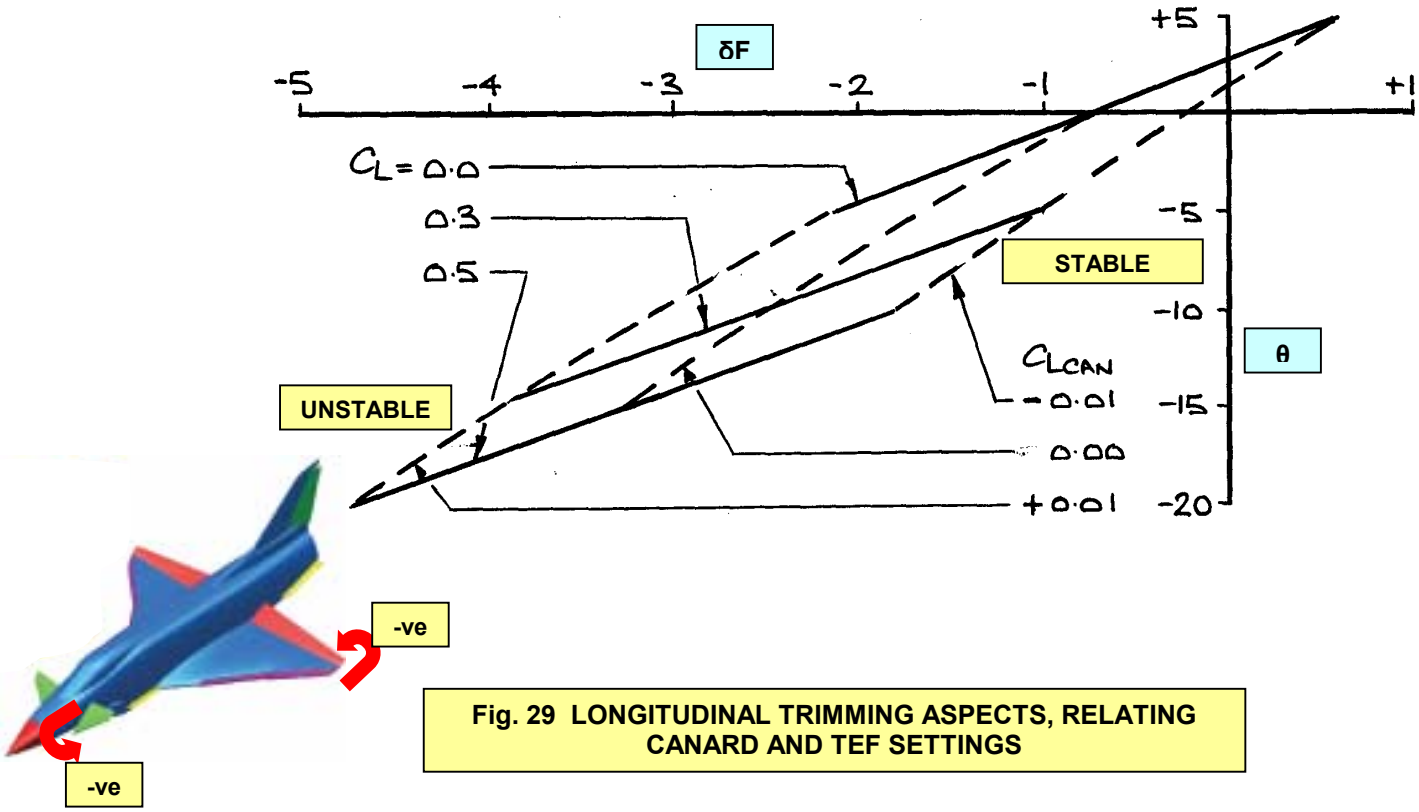

Fig. 29 LONGITUDINAL TRIMMING ASPECTS, RELATING CANARD AND TEF SETTINGS

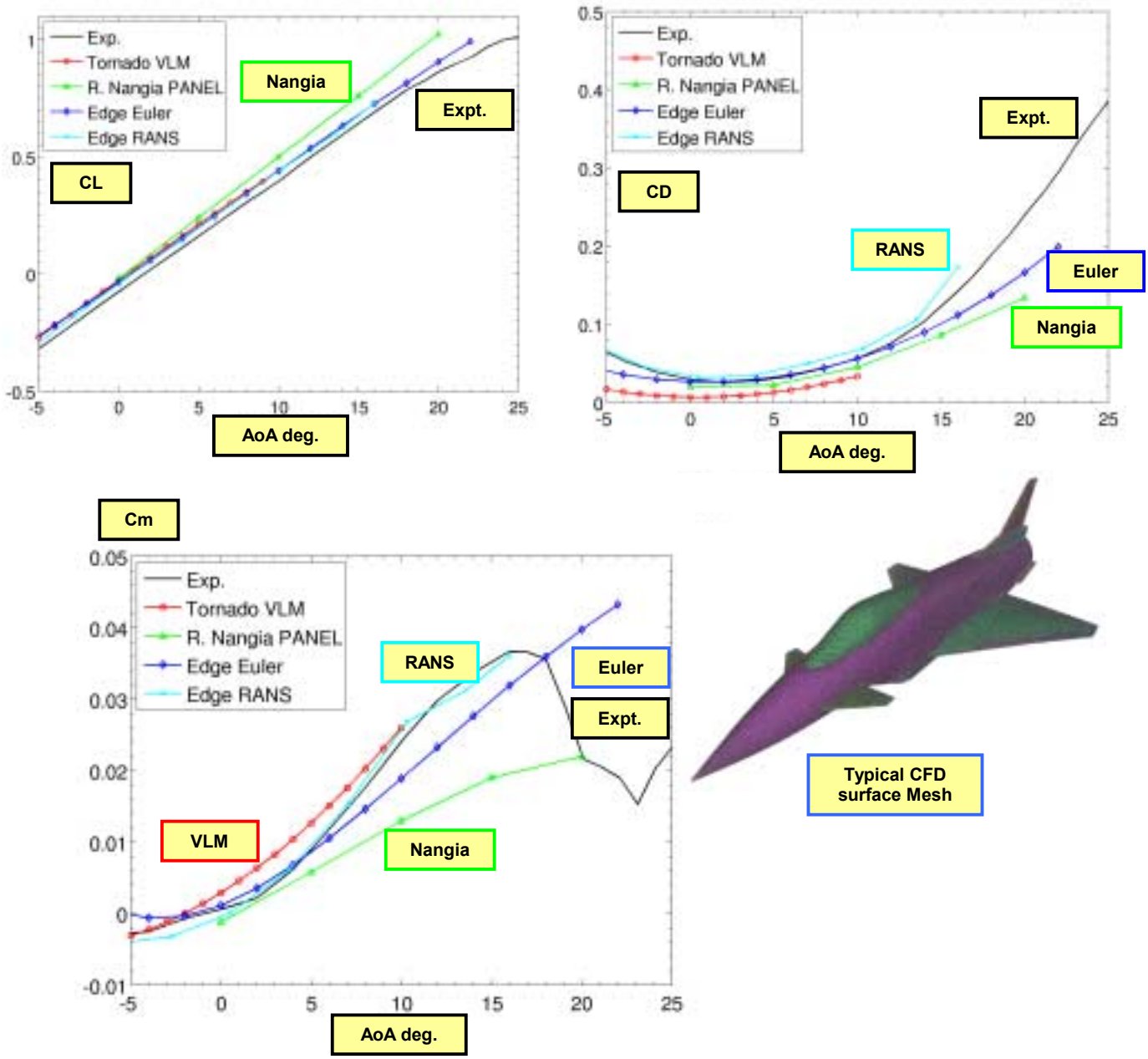

FIG. 30 FULL CONFIGURATION, FORCE & MOMENT COEFFICIENT VARIATIONS, RECENT COMPARATIVE RESULTS FROM REF.8